Imaging Localized Energy States in Silicon-Doped InGaN Nanowires Using 4D Electron Microscopy

Riya Bose,[†] *Aniruddha Adhikari,*[†] *Victor M. Burlakov,*[‡] *Guangyu Liu,*[ǀ] *Azimul Mohammed,*[ǂ] *Davide Priante,*[ǀ] *Mohamed N. Hedhili,*[#] *Nimer Wehbe,*[#] *Chao Zhao,*[ǀ] *Haoze Yang,*[†] *Tien Khee Ng,*[ǀ] *Alain Goriely,*[‡] *Osman M. Bakr,*[†] *Tom Wu,*[ǂ] *Boon S. Ooi,*[ǀ] *Omar F. Mohammed*[†*]

[†]KAUST Solar Center, Physical Sciences and Engineering Division, King Abdullah University of Science and Technology, Thuwal 23955-6900, Kingdom of Saudi Arabia

[‡]Mathematical Institute, University of Oxford, Woodstock Road, Oxford OX2 6GG, UK

[ǀ]Photonics Laboratory, Computer, Electrical, and Mathematical Sciences and Engineering KAUST, Thuwal, 23955-6900, Kingdom of Saudi Arabia

[ǂ]Physical Sciences and Engineering Division, King Abdullah University of Science and Technology, Thuwal 23955-6900, Kingdom of Saudi Arabia

[#]Imaging and Characterization Laboratory, King Abdullah University of Science and Technology, Thuwal 23955-6900, Saudi Arabia

ABSTRACT. InGaN nanowires (NWs) are unique building blocks found in several types of semiconductor-based optoelectronic devices. Introducing dopants into such NWs is known to

significantly improve the device performances through a variety of mechanisms. However, to further optimize device operation, a precise knowledge of ultrafast dynamical processes at the surface and interface of these NWs is imperative. Accessing such surface dynamics selectively is a capability that has been beyond the reach of any time-resolved laser spectroscopy with optical detection to date, due to the relatively large penetration depth of photon pulses. Here, we describe the development of four-dimensional scanning ultrafast electron microscopy (4D S-UEM) as an extremely surface-sensitive method to directly visualize in space and time the tremendous impact of silicon doping on the surface-carrier dynamics of InGaN nanowires. More specifically, we found that the introduction of dopant-induced trap states clearly dictates and controls the overall secondary electron injection and charge carrier dynamics. Interestingly, two time regime dynamics are identified for the first time in a 4D S-UEM experiment: an early time behavior (within 200 picoseconds) associated with the delayed evolution of secondary electrons due to the presence of localized trap states that decrease the electron escape rate and a longer timescale behavior (few ns) marked by accelerated charge carrier recombination. We also found that the rates of both these phenomena strongly depend on the Si-dopant concentration and are markedly different from those of the undoped analogue. The results are further corroborated by conductivity studies carried out under dark and illumination. These new findings will help to enhance the performance of these nanowires in optoelectronic devices and other state-of-the-art devices that rely on surface and interfacial charge carrier dynamics.

KEYWORDS. 4D scanning ultrafast electron microscopy, doping, charge carrier dynamics, trap states, InGaN, Si doped, secondary electron dynamics

The dynamics of charge carriers at material surfaces and interfaces not only plays a pivotal role in controlling the applicability of nanoscale materials to any optoelectronic or microelectronic devices, but also is one of the major challenges in the development of these real-world energy devices. However, real-space and real-time mapping of charge carrier dynamics selectively at material surfaces is beyond the reach of any conventional static spectroscopic or microscopic methods and has only been possible due to recent development of four-dimensional scanning ultrafast electron microscopy (4D S-UEM).[1-10] This technique relies on using photoelectron packets to probe the secondary electrons (SEs) generated from the first few nanometers of the top surface of the material as a result of the interaction of the electron beam with the surface of the photoactive material, thus opening up a new dimension in imaging techniques: observing the change in charge carrier dynamics explicitly at the surface of the sample in real space and time.

Several approaches have been developed to manipulate charge carrier dynamics in order to enhance the device functionality of many photoactive materials; doping being one of the most effective ways among them.[11-21] In general, insertion of foreign ions leads to the formation of additional levels in the bandgap of the host material that not only provide additional relaxation routes for the charge carriers, but also may alter the density of states and the band structure, which result in significant changes in both the optical and electronic properties of the host material. For example, group III nitride semiconductors, in particular ternary InGaN nanowires (NWs), have gained much attention because of their widespread application as the building block for diverse optoelectronic and photoelectrochemical devices,[17-20,22-25] stemming from their photostability and widely tunable direct bandgap from the near UV to near IR regions (3.4 eV-0.7 eV), along with the suitability of the nanowire geometry to allow strain-relaxed growth of

complex heterostructures.[26-29] To further enhance the efficiencies of InGaN-based devices, Si has been introduced as an n-dopant, that is reported to affect the growth process of NWs, leading to a reduction in structural defects, improvement in their morphology and interface quality, as well as an increase in their thermal stability.[30-33] Most importantly, Si doping can tune the charge carrier dynamics by altering the band structure and carrier recombination.[25,34,35] Moreover, Si doping leads to screening of the internal piezoelectric field, which in turn reduces the quantum-confined Stark effect, resulting in the decrease of carrier localization, increased PL emission intensity and lower threshold power density for obtaining stimulated emission.[34,36-38]

Although efforts have been made to employ 4D S-UEM to monitor the surface charge carrier dynamics of a few technologically important materials, the effect of doping, which is a huge factor in the optoelectronic properties of the host material, on the SE dynamics remains unexplored. Herein, we investigate the effect of Si doping on the surface charge carrier and SE dynamics of InGaN/GaN NWs using 4D S-UEM. Faster SE kinetics are observed for the Si-doped NWs; however, the growth of the SE signal in the first hundred picosecond regime becomes slower as the Si dopant concentration increases. To understand such an anomaly in the SE kinetics in two different time regions, we conducted a theoretical investigation and determined that the delay in the contrast evolution of the doped samples can be ascribed to the presence of localized trap states originated from doping, which decrease the electronic escape rate, whereas the decay in dark contrast arises from energy losses of the secondary electrons due to their interaction with free and localized carriers generated by dopants. This behavior is also manifested in the photoconductivity of the doped and undoped NWs, where the doped NWs show a decrease in the conductivity upon illumination because of the scattering phenomenon as the charge carrier concentration increases. The current study provides detailed experimental and

theoretical insight into the impact of doping on the charge carrier dynamics and electronic properties of InGaN NWs, which will pave the way to further optimize their properties.

The samples of InGaN/GaN NWs are grown on Si substrate by a plasma-assisted molecular beam epitaxy method.[8,39] It has already been reported that the use of GaN NWs as templates instead of direct growth of InGaN on Si substrate leads to improved structural properties.[25] For doping the NWs with Si, two different temperatures are used in order to vary the concentration of the dopant ions, with the higher temperature resulting in a higher dopant concentration. Details of the NW growth procedure are described in the Experimental section.

Figure 1a shows a dark field TEM image of the NWs confirming the formation of the heterostructure and Figure 1(b-d) show the corresponding cross-sectional scanning electron microscopy (SEM) images. The length and the width of the NWs vary in the ranges of ~220-240 nm and ~20-30 nm, respectively, and they do not change with doping.

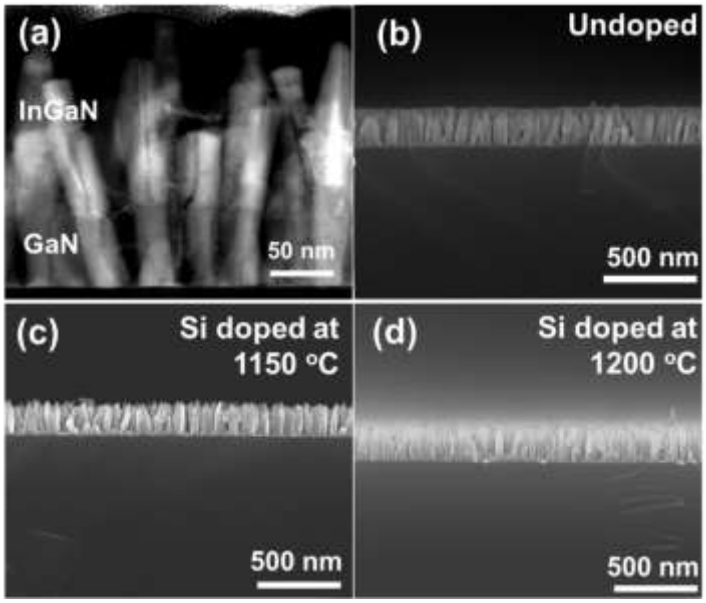

Figure 1. (a) Dark-field TEM image of the InGaN/GaN heterostructures where different image contrast between the GaN and InGaN parts is observed, confirming the formation of

heterostructures and (b-d) cross-sectional SEM images of the undoped NWs, NWs doped with Si at 1150 °C and NWs doped with Si at 1200 °C, respectively. Top-view SEM images of the NWs are provided in the Supporting information (Figure S1).

Figure 2 shows the time-resolved 4D S-UEM difference images of the undoped and doped NWs. The S-UEM technique relies on detecting the changes in the secondary electrons emitted from the top few nanometers of the material surfaces followed by optical excitation and probing with a pulsed electron beam, thus precisely revealing the dynamics of the charge carriers on the surface of the material. A schematic diagram of the 4D S-UEM setup is provided in Figure S2 of the Supporting information; detailed information on the principle of its operation has been published elsewhere.[1,6] Briefly, S-UEM combines the output of a fs Clark-MXR fiber laser system with a modified Quanta FEI-650 SEM. The fundamental output of the laser centered at 1030 nm (pulse, ~270 fs pulse duration and 200 kHz to 25.4 MHz repetition rate) is split by a 1:1 beam splitter to pump two second/third harmonic generators (HG, Clark-MXR) simultaneously to produce 515 and 343 nm pulses. The 343 nm output is focused onto the Schottky field emitter tip inside the SEM to generate the pulsed electrons, which are then accelerated towards the sample using 30 kV voltage. The 515 nm output enters the microscope through a viewport at a 50-degree angle relative to the surface normal and delivers the excitation clocking pulse to the sample. The scanning process of the electron beam proceeds across the surface of the sample, both the laser excited and unexcited regions, in a raster pattern, and the secondary electrons (SEs) emitted from the sample are detected by a positively biased Everhart-Thornley detector. The SE images are obtained at different time delays between the electron and optical pulses as an integration of 64 frames with a dwell time of 300 ns at each pixel to improve the signal-to-noise ratio. Finally, all experiments are conducted at a repetition rate of 8 MHz to

ensure full recovery of the specimen before the arrival of the next pulse. Contrast-enhanced differences in the SE images from the laser (pump pulse)-irradiated and non-irradiated regions are then extracted with reference to a negative time frame before the arrival of the excitation photon pulse. The evolution of the dark contrast with time for all the samples in the laser illuminated region suggests that while traveling towards the surface, the photogenerated SEs lose their energy through scattering events; hence, fewer of them are detected by the detector compared to an unilluminated specimen. A similar observation has already been reported for InGaN NWs and GaAs.[3,8,40] Dense packing of the NWs enables the carrier diffusion across the boundaries of the NWs, and hence, the SE signal spreads beyond the laser-illuminated area.[3,8]

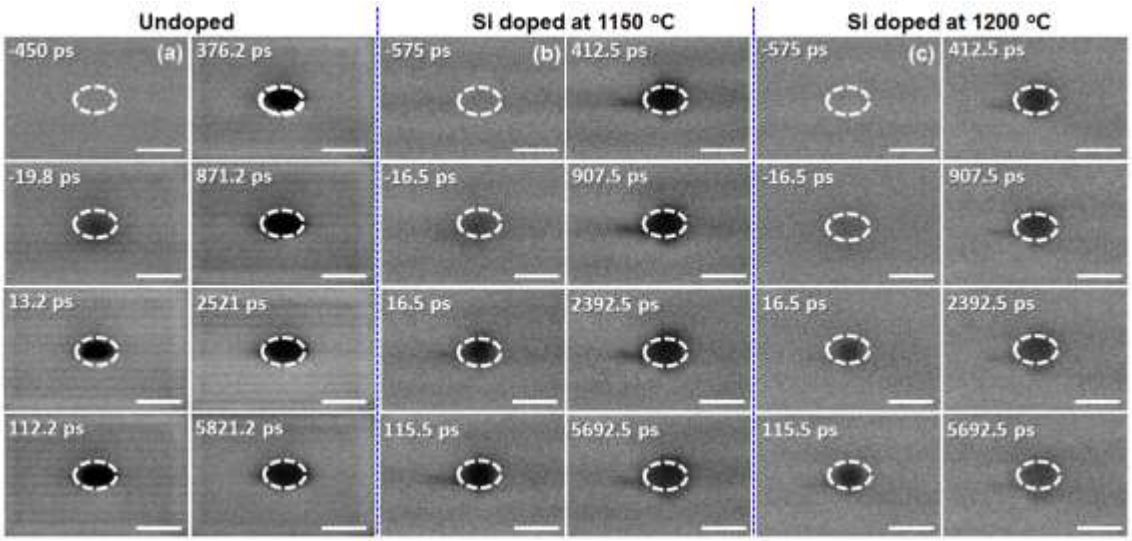

Figure 2. Time-resolved SE difference images at indicated time delays for (a) undoped and (b-c) Si-doped NWs at an excitation wavelength of 515 nm. The dark circle indicates the laser footprint on the sample. No change in the image contrast is observed at the far negative time delays, indicating the recovery of the system to the initial state after each pump−probe event. The scale bar is 50 μm.

Plotting the SE intensity changes from the center of the laser excitation footprint as a function of the time delays reveals that Si doping results in faster fading away of the dark SE signal, indicating faster carrier relaxation in doped samples (Figure 3a). One plausible reason is an increase in the number of scattering events in the Si-doped samples because of the increase in the carrier concentration with doping. Reduction in the emission decay lifetime of InGaN emitters with Si doping has also been reported in the literature and has been attributed to screening of the quantum-confined Stark effect and increases in the electron-hole wave function overlap after doping.[41,42] Surprisingly, zooming into the SE kinetics at a very early timescale (~200 ps) reveals slower growth of the dark signal in the doped samples than in the undoped one (Figure 3b). This effect becomes even more prominent as the concentration of the Si dopant increases.

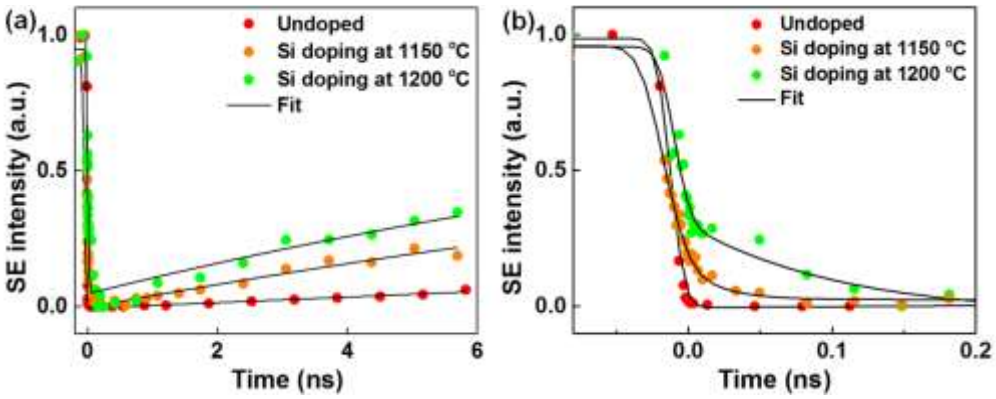

Figure 3. Dynamics of the temporal evolution of the SE intensity at the center of the laser footprint region (a) on 6 ns time scale and (b) zoomed-in view in the first 200 ps regime.

Considering the total length of GaN and InGaN NWs, which is much smaller (~0.25 μm) than that of the Si substrate (350-400 μm), the Fermi level at equilibrium is determined by the thickness of the doped Si substrate. Indeed, even if we assume that a compact layer of 0.25 μm thickness on the doped Si substrate is doped up to 10^{20} cm^{-3} and injects all the electrons into Si,

which has a much lower Fermi level, the concentration of carriers in the substrate would grow by $6 \div 7 \cdot 10^{16}$ cm^{-3}. The latter case is probably less than 10% of the initial carrier concentration in the doped Si substrate. This means that the Fermi level of the substrate would roughly stay at the same position upon NW growth, while the Fermi levels in the GaN and InGaN NWs would decrease down to level up with that in the substrate. This conclusion is even more appropriate when taking into account the fact that only a fraction of the free electrons can be injected from the NWs into the substrate. Plotting the band diagrams in the undoped and doped (Figure 4a and 4b, Figure S3-5) cases shows that there is very little difference between the two; hence, the band bending is unlikely to be a reason for the observed change in the time evolution of the dark contrast (Figure 3).

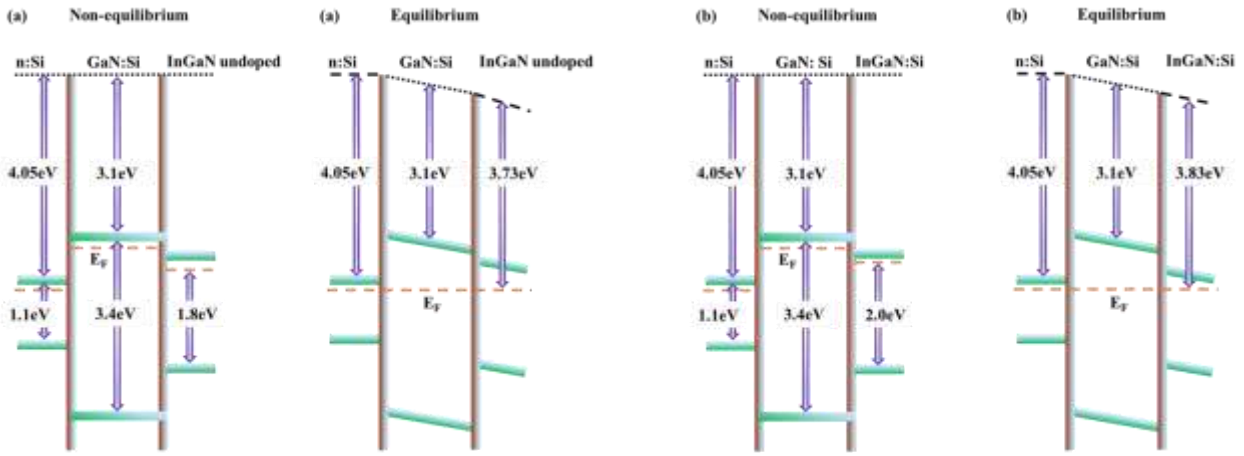

Figure 4. Flat band diagrams for (a) Si substrate-Si:GaN-InGaN and (b) Si substrate-Si:GaN-Si:InGaN under both equilibrium and non-equilibrium conditions.

The slower growth of the dark contrast in the doped InGaN NWs (see Figure 3b) could be due to the presence of localized energy levels associated with Si doping of the InGaN nanowires.

These localized levels can trap electrons, and their occupancy at equilibrium depends on the trapping energy, the total concentrations of free and trapped electrons and the sample temperature. Interaction of the secondary electrons generated by the probe electron pulse with the free and trapped electrons in Si:InGaN can be significantly different. For example, this interaction with the trapped electrons can be more substantial, in which case the trapping dynamics of the photogenerated electrons would be observed as a delayed growth of the dark contrast (DC).

The trap states can also promote electron-hole recombination, which normally occurs on a longer time scale than the DC growth, namely, a few hundred nanoseconds. This effect would then be observed as a quicker recovery of the dark contrast. The occupancy of the trap states in this case can be considered to be in quasi-equilibrium with the free electrons. Below, we present a theoretical framework for describing the slower growth and quicker decay of the dark contrast in Si-doped InGaN NWs than in the undoped InGaN. In summary, the trap states introduced by Si doping appear to influence different phenomena occurring in different time windows: delayed SE emission (~200 ps) but accelerated carrier recombination (several ns).

Evolution of the photogenerated carriers can be described by kinetic equations for the concentration of localized (trapped) n_L electrons and the concentration n_g of generated electrons (and holes)

$$\begin{aligned} \frac{dn_L}{dt} &= \sigma_{trap} \cdot \left(n_g + n_b - n_L\right) \cdot \left(N_L - n_L\right) - n_L \cdot r_{esc} - \gamma_L n_L n_g \\ \frac{dn_g}{dt} &= -\gamma_L n_L n_g - \gamma_f \left(n_b + n_b - n_L\right) \cdot n_g \end{aligned} \tag{1}$$

where n_b is the background concentration of electrons (n-doping); N_L is the concentration of dopants (localized states); σ_{trap} and r_{esc} are the trapping and detrapping (escape) rates,

respectively; and γ_L and γ_f are the recombination rates for the trapped and free electrons, respectively. According to the experimental data on DC time evolution, the characteristic time scales for the DC growth and subsequent decay are very different. In particular, DC growth occurs within a fraction of a nanosecond, while the decay takes significantly longer, namely, definitely more than 10 ns. This suggests that the growth and the decay kinetics of the DC can be analyzed independently.

Summarizing both the growth and decay of the DC as detailed in the supporting information and transforming the equations to mimic the dependences shown in Figure 3 provide

$$\begin{aligned} I_{DC}(t) &= P_1 \cdot \left[P_2 \cdot N_L \cdot \left(1 - \exp\left(-r_{esc} \cdot t\right)\right) + 1 \right] + 1 \quad \textit{rise} \\ I_{DC}(t) &= P_1 \cdot \left[P_2 \cdot N_L + 1 \right] \cdot \exp\left(-\Gamma \cdot N_L \cdot t\right) + 1 \quad \textit{decay} \\ P_1 &= \frac{n_g(0)\sigma_f}{P_2 \cdot N_L + 1},\ P_2 = \left(\sigma_L - \sigma_f\right) \cdot \frac{\sigma_{trap}}{\sigma_f \cdot r_{esc}} \end{aligned} \tag{2}$$

As we can see from these expressions, the decay rate is proportional to N_L, suggesting a faster decay at higher dopant concentrations, which is exactly what is observed experimentally (see Figure 3a). The DC growth and decay simulated using Eqs (2) are shown in Figure 5 for $n_g(0)\sigma_f = -1$, $P_2 = 5 \cdot 10^{-21}\, cm^3$, $r_{esc} = 20\, ns^{-1}$, $\Gamma = 5 * 10^{-22}\, ns^{-1} cm^3$ and various N_L values.

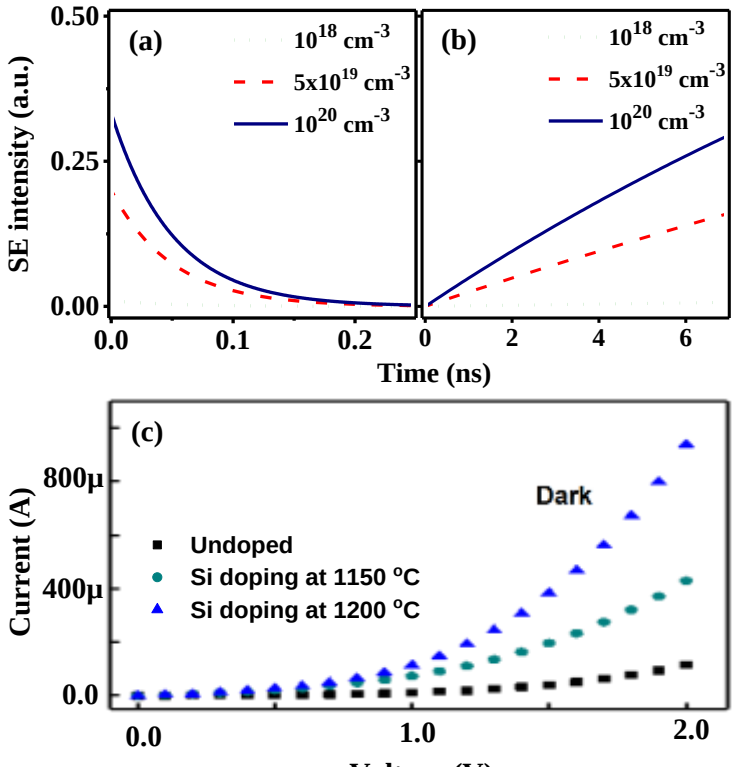

Figure 5. Time dependences of secondary electron intensity (dark contrast) after the photoexcitation of the samples: (a) growth and (b) decay. The values of N_L are 10^{18} cm^{-3} (dotted line), $5*10^{19}$ cm^{-3} (dashed line), and 10^{20} cm^{-3} (solid line). (c) Comparison of the dark current for the undoped and Si-doped InGaN/GaN NW devices.

By comparing Figures 3 and 5, we find a good qualitative agreement between the theory and experimental data. This indicates that our assumption about the role of the localized energy levels in changing the time evolution of the DC can be quite appropriate. Accordingly, we can estimate the content of Si doping in InGaN NWs at higher temperature: most likely, it results in an increase in the dopant concentration (N_L) by approximately a factor of 2.

We further carried out electrical characterization to understand the effect of the same factor on the photoresponse of the material. As shown in Figure 5c, the dark current of the Si-doped samples is higher than that of the undoped one, which is consistent with the fact that the doped samples have a higher carrier concentration. Under illumination, the undoped sample (Figure S6a) exhibited a typical photoresponse (a decrease in resistance under illumination). Interestingly, the photoresponse of the doped samples is to some extent opposite: the resistance *slightly increases* under illumination, and the effect increases with increasing Si dopant concentration (Figure S6(b-c)). This can be attributed to carrier-carrier scattering due to the high carrier concentration in the case of the Si-doped samples, which is consistent with the secondary electron dynamics observed from 4D S-UEM. Similar observations (a decrease in conductivity under illumination) have already been reported for other semiconductor devices.[43-47]

By omitting the effects of the electric-field dependence resulting in the non-linear growth of the current, we focus on only the sign of the conductivity change under illumination. Consider the generic expression for the electrical conductivity of a material

$$\sigma = e \cdot \left(n_e \mu_e + n_h \mu_h \right) \tag{3}$$

where e is electronic charge; n_e and n_h are the concentrations of electrons and holes, respectively; and μ_e and μ_h are their corresponding mobilities. It is known that electron mobility is much higher than that of holes; therefore, for the purpose of demonstration, we neglect the hole mobility. The electron mobility can be written by explicitly showing the carrier-carrier interactions as

$$\mu_e = \frac{e}{m} \cdot \tau_e = \frac{e}{m} \cdot \frac{1}{\left(\gamma_0 + \gamma_1 n_e + \gamma_e n_h \right)} \tag{4}$$

where γ_0, γ_1 and γ_2 are the (positive) rates of electronic scattering for defects (and impurities), electrons and holes, respectively. We are interested in the change in the conductivity given by Eq (3) by taking into account Eq (4) under illumination. This generates extra concentrations $\delta n << n_e$ of electrons and holes, and recalling that for n-doped samples, $n_h = 0$

$$\begin{aligned} \Delta\sigma &= \sigma_{light} - \sigma_{dark} \\ &= \frac{e^2}{m} \frac{\left(n_e + \delta n \right)}{\left(\gamma_0 + \gamma_1 \left(n_e + \delta n \right) + \gamma_2 \delta n \right)} - \frac{e^2}{m} \frac{n_e}{\left(\gamma_0 + \gamma_1 n_e \right)} = \frac{e^2}{m} \cdot \left(\frac{\delta n \left(\gamma_0 - \gamma_2 n_e \right)}{\left(\gamma_0 + \gamma_1 \left(n_e + \delta n \right) + \gamma_2 \delta n \right) \cdot \left(\gamma_0 + \gamma_1 n_e \right)} \right) \end{aligned} \tag{5}$$

This expression shows that the photoinduced change in conductivity is always positive for an undoped sample, as $n_e \approx 0$. It also shows that $\Delta\sigma$ can be negative for sufficiently high doping when $\gamma_0 < \gamma_2 n_e$, i.e., if the scattering of background electrons with photogenerated electrons is high enough. In conclusion, the effect of illumination has two competing contributions: the one due to the increase in charge carrier concentration is positive, and the other one due to the

increased scattering of carriers is negative. The latter contribution may dominate for heavily doped samples, as in the case of the specimens we have studied.

To conclude, we observe the effect of Si doping on the surface charge carrier dynamics of Si-doped InGaN NWs by 4D S-UEM. An interesting behavior of SE contrast evolution is observed, where there is a delay in the dark contrast evolution in the fast time regime for the doped samples; however, on a longer time scale, the doped samples show faster decay of the SE signal. To understand such behavior, we opted for a theoretical study, which reveals the presence of localized trap states with Si doping that lead to a slower electron release rate and hence a slower growth of the SE signal, whereas on a longer time scale, the scattering of the secondary electron beam with an increased number of charge carriers in the doped samples leads to a faster decay of SE signal. This behavior is also manifested in the photoconductivity of the NWs, whereas the doped NWs show an increase in resistance with illumination because of carrier scattering. This study provides a detailed understanding of the impact of Si doping on the charge carrier dynamics of InGaN NWs and will help to further optimize their properties.

Experimental Section

Fabrication of NWs:

The InGaN nanowires were grown on 3-inch diameter phosphorus-doped silicon (100) substrate using Plasma Assisted Molecular Beam Epitaxy system (PAMBE, Veeco GEN930). The substrate has a resistivity of 0.01-0.02 ohm·cm, and was first cleaned with 20% hydrofluoric acid to remove the native oxide. Outgassing was performed in both load-lock and buffer chambers for 1 hour at 200°C and 2 hours at 600°C respectively. The substrate was then loaded in the ultra-high vacuum growth chamber. The Si-doped GaN layer was first grown at 680°C with a Ga

beam equivalent pressure (BEP) of 5e-8 Torr. Following, the temperature was reduced to 508°C to grow InGaN with a In BEP fixed at 1.5e-8 Torr and Ga BEP of 3.1 e-8 Torr. The high-brightness N2 plasma was sustained using a flow rate of 1 sccm and RF power of 350 W.

ASSOCIATED CONTENT

Supporting Information. Instrumentation, device fabrication procedure, detailed theoretical calculation and supporting figures. This material is available free of charge via the Internet at http://pubs.acs.org

AUTHOR INFORMATION

Corresponding Author

*Email. omar.abdelsaboor@kaust.edu.sa

REFERENCES

1. Mohammed, O. F.; Yang, D.-S.; Pal, S. K.; Zewail, A. H., *J. Am. Chem. Soc.* **2011**, *133*, 7708-7711.

2. Bose, R.; Ahmed, G. H.; Alarousu, E.; Parida, M. R.; Abdelhady, A. L.; Bakr, O. M.; Mohammed, O. F., *J. Phys. Chem. C* **2015**, *119*, 3439-3446.

3. Khan, J. I.; Adhikari, A.; Sun, J.; Priante, D.; Bose, R.; Shaheen, B. S.; Ng, T. K.; Zhao, C.; Bakr, O. M.; Ooi, B. S.; Mohammed, O. F., *Small* **2016**, *12*, 2313-2320.

4. Adhikari, A.; Eliason, J. K.; Sun, J.; Bose, R.; Flannigan, D. J.; Mohammed, O. F., *ACS Appl. Mater. Interfaces* **2017**, *9*, 3-16.

5. Sun, J.; Adhikari, A.; Shaheen, B. S.; Yang, H.; Mohammed, O. F., *J. Phys. Chem. Lett.* **2016**, *7*, 985-994.

6. Sun, J.; Melnikov, V. A.; Khan, J. I.; Mohammed, O. F., *J. Phys. Chem. Lett.* **2015**, *6*, 3884-3890.

7. Bose, R.; Bera, A.; Parida, M. R.; Adhikari, A.; Shaheen, B. S.; Alarousu, E.; Sun, J.; Wu, T.; Bakr, O. M.; Mohammed, O. F., *Nano Lett.* **2016**, *16*, 4417-4423.

8. Bose, R.; Sun, J.; Khan, J. I.; Shaheen, B. S.; Adhikari, A.; Ng, T. K.; Burlakov, V. M.; Parida, M. R.; Priante, D.; Goriely, A.; Ooi, B. S.; Bakr, O. M.; Mohammed, O. F., *Adv. Mater.* **2016**, *28*, 5106-5111.

9. Yang, D.-S.; Mohammed, O. F.; Zewail, A. H., *Proc. Natl. Acad. Sci.* **2010**, *107*, 14993-14998.

10. Shaheen, B. S.; Sun, J.; Yang, D.-S.; Mohammed, O. F., *J. Phys. Chem. Lett.* **2017**, *8*, 2455-2462.

11. Erwin, S. C.; Zu, L.; Haftel, M. I.; Efros, A. L.; Kennedy, T. A.; Norris, D. J., *Nature* **2005**, *436*, 91-94.

12. Norris, D. J.; Efros, A. L.; Erwin, S. C., *Science* **2008**, *319*, 1776-1779.

13. Mocatta, D.; Cohen, G.; Schattner, J.; Millo, O.; Rabani, E.; Banin, U., *Science* **2011**, *332*, 77.

14. Arkhipov, V. I.; Heremans, P.; Emelianova, E. V.; Bässler, H., *Phys. Rev. B* **2005**, *71*, 045214.

15. Berggren, K. F.; Sernelius, B. E., *Phys. Rev. B* **1981**, *24*, 1971-1986.

16. Abram, R. A.; Rees, G. J.; Wilson, B. L. H., *Adv. Phys.* **1978**, *27*, 799-892.

17. Koester, R.; Hwang, J.-S.; Salomon, D.; Chen, X.; Bougerol, C.; Barnes, J.-P.; Dang, D. L. S.; Rigutti, L.; de Luna Bugallo, A.; Jacopin, G.; Tchernycheva, M.; Durand, C.; Eymery, J., *Nano Lett.* **2011**, *11*, 4839-4845.

18. Shuji, N.; Masayuki, S.; Shin-ichi, N.; Naruhito, I.; Takao, Y.; Toshio, M.; Hiroyuki, K.; Yasunobu, S., *Jpn. J. Appl. Phys.* **1996**, *35*, L74.

19. Chuang, R. W.; Chang, S. P.; Chang, S. J.; Chiou, Y. Z.; Lu, C. Y.; Lin, T. K.; Lin, Y. C.; Kuo, C. F.; Chang, H. M., *J. Appl. Phys.* **2007**, *102*, 073110.

20. Dong, Y.; Tian, B.; Kempa, T. J.; Lieber, C. M., *Nano Lett.* **2009**, *9*, 2183-2187.

21. Begum, R.; Parida, M. R.; Abdelhady, A. L.; Murali, B.; Alyami, N. M.; Ahmed, G. H.; Hedhili, M. N.; Bakr, O. M.; Mohammed, O. F., *J. Am. Chem. Soc.* **2017**, *139*, 731-737.

22. Kim, H.-M.; Cho, Y.-H.; Lee, H.; Kim, S. I.; Ryu, S. R.; Kim, D. Y.; Kang, T. W.; Chung, K. S., *Nano Lett.* **2004**, *4*, 1059-1062.

23. Tchernycheva, M.; Messanvi, A.; de Luna Bugallo, A.; Jacopin, G.; Lavenus, P.; Rigutti, L.; Zhang, H.; Halioua, Y.; Julien, F. H.; Eymery, J.; Durand, C., *Nano Lett.* **2014**, *14*, 3515-3520.

24. Hwang, Y. J.; Wu, C. H.; Hahn, C.; Jeong, H. E.; Yang, P., *Nano Lett.* **2012**, *12*, 1678-1682.

25. AlOtaibi, B.; Nguyen, H. P. T.; Zhao, S.; Kibria, M. G.; Fan, S.; Mi, Z., *Nano Lett.* **2013**, *13*, 4356-4361.

26. Kuykendall, T.; Ulrich, P.; Aloni, S.; Yang, P., *Nat Mater* **2007**, *6*, 951-956.

27. Yam, F. K.; Hassan, Z., *Superlattices Microstruct.* **2008**, *43*, 1-23.

28. Takashi, M.; Motokazu, Y.; Shuji, N., *Jpn. J. Appl. Phys.* **1999**, *38*, 3976.

29. Yan, R.; Gargas, D.; Yang, P., *Nat. Photon.* **2009**, *3*, 569-576.

30. Kamimura, J.; Ramsteiner, M.; Geelhaar, L.; Riechert, H., *J. Appl. Phys.* **2014**, *116*, 244310.

31. Chen, M.-K.; Cheng, Y.-C.; Chen, J.-Y.; Wu, C.-M.; Yang, C. C.; Ma, K.-J.; Yang, J.-R.; Rosenauer, A., *J. Cryst. Growth* **2005**, *279*, 55-64.

32. Lee, S.-N.; Kim, J.; Kim, K.-K.; Kim, H.; Kim, H.-K., *J. Appl. Phys.* **2010**, *108*, 102813.

33. Li, D.-B.; Katsuno, T.; Nakao, K.; Aoki, M.; Miyake, H.; Hiramatsu, K., *J. Cryst. Growth* **2006**, *290*, 374-378.

34. Wang, Y. J.; Xu, S. J.; Li, Q.; Zhao, D. G.; Yang, H., *Appl. Phys. Lett.* **2006**, *88*, 041903.

35. Zhao, S.; Fathololoumi, S.; Bevan, K. H.; Liu, D. P.; Kibria, M. G.; Li, Q.; Wang, G. T.; Guo, H.; Mi, Z., *Nano Lett.* **2012**, *12*, 2877-2882.

36. Davies, M. J.; Dawson, P.; Massabuau, F. C. P.; Oliver, R. A.; Kappers, M. J.; Humphreys, C. J., *Appl. Phys. Lett.* **2014**, *105*, 092106.

37. Chiaki, S.; Fumito, M.; Tomoaki, K.; Masahide, K.; Yasuhiro, M.; Yuji, A.; Atsushi, A. Y., *Jpn. J. Appl. Phys.* **2013**, *52*, 115601.

38. Chichibu, S.; Cohen, D. A.; Mack, M. P.; Abare, A. C.; Kozodoy, P.; Minsky, M.; Fleischer, S.; Keller, S.; Bowers, J. E.; Mishra, U. K.; Coldren, L. A.; Clarke, D. R.; DenBaars, S. P., *Appl. Phys. Lett.* **1998**, *73*, 496-498.

39. Guo, W.; Zhang, M.; Banerjee, A.; Bhattacharya, P., *Nano Lett.* **2010**, *10*, 3355-3359.

40. Cho, J.; Hwang, T. Y.; Zewail, A. H., *Proc. Natl. Acad. Sci.* **2014**, *111*, 2094-2099.

41. Milan , S. M.; Shigefusa, C.; Siegfried , B. F.; Amber , C. A.; John , E. B.; Evelyn , L. H.; Stacia, K.; Umesh , K. M.; Steven , P. D., *Jpn. J. Appl. Phys.* **1998**, *37*, L1362.

42. Cho, Y.-H.; Song, J. J.; Keller, S.; Minsky, M. S.; Hu, E.; Mishra, U. K.; DenBaars, S. P., *Appl. Phys. Lett.* **1998**, *73*, 1128-1130.

43. Wang, M.; Ren, F.; Zhou, J.; Cai, G.; Cai, L.; Hu, Y.; Wang, D.; Liu, Y.; Guo, L.; Shen, S. N. **2015**, *5*, 12925.

44. Tyler, W. W.; Woodbury, H. H., *Phys. Rev.* **1956**, *102*, 647-655.

45. Jensen, S. A.; Mics, Z.; Ivanov, I.; Varol, H. S.; Turchinovich, D.; Koppens, F. H. L.; Bonn, M.; Tielrooij, K. J., *Nano Lett.* **2014**, *14*, 5839-5845.

46. Wei, P.-C.; Chattopadhyay, S.; Yang, M.-D.; Tong, S.-C.; Shen, J.-L.; Lu, C.-Y.; Shih, H.-C.; Chen, L.-C.; Chen, K.-H., *Phys. Rev. B* **2010**, *81*, 045306.

47. Höpfel, R. A.; Shah, J.; Wolff, P. A.; Gossard, A. C., *Phys. Rev. B* **1988**, *37*, 6941-6954.

Table of Contents Graphic